

# Striking Isotopologue-Dependent Photodissociation Dynamics of Water Molecules: The Signature of an Accidental Resonance

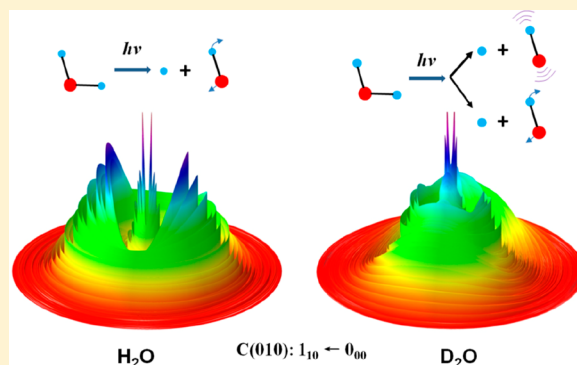
Yao Chang,<sup>†,§</sup> Zhichao Chen,<sup>†,§</sup> Jiami Zhou,<sup>†</sup> Zijie Luo,<sup>†</sup> Zhigang He,<sup>†</sup> Guorong Wu,<sup>\*,†,‡</sup> Michael N. R. Ashfold,<sup>‡</sup> Kaijun Yuan,<sup>\*,†,‡</sup> and Xueming Yang<sup>\*,†</sup>

<sup>†</sup>State Key Laboratory of Molecular Reaction Dynamics, Dalian Institute of Chemical Physics, Chinese Academy of Sciences, 457 Zhongshan Road, Dalian 116023, China

<sup>‡</sup>School of Chemistry, University of Bristol, Bristol BS8 1TS, United Kingdom

## Supporting Information

**ABSTRACT:** Investigations of the photofragmentation patterns of both light and heavy water at the state-to-state level are a prerequisite for any thorough understanding of chemical processing and isotope heterogeneity in the interstellar medium. Here we reveal dynamical features of the dissociation of water molecules following excitation to the  $\tilde{C}(010)$  state using a tunable vacuum ultraviolet source in combination with the high-resolution H(D)-atom Rydberg tagging time-of-flight technique. The action spectra for forming H(D) atoms and the OH(OD) product state distributions resulting from excitation to the  $\tilde{C}(010)$  states of H<sub>2</sub>O and D<sub>2</sub>O both show striking differences, which are attributable to the effects of an isotopologue-specific accidental resonance. Such accidental-resonance-induced state mixing may contribute to the D/H isotope heterogeneity in the solar system. The present study provides an excellent example of competitive state-to-state nonadiabatic decay pathways involving at least five electronic states.



Water, ubiquitous in the universe, absorbs light at all wavelengths ( $\lambda$ ) in the vacuum ultraviolet (VUV) region below 190 nm,<sup>1</sup> resulting in fragmentation leading to a hydrogen (H) atom and a hydroxyl (OH) radical or, at shorter wavelengths, the three constituent atoms. The single bond fission process is an important source of OH radicals in the interstellar medium (ISM).<sup>2,3</sup> An in-depth understanding of the OH product quantum-state population distributions from the photodissociation of water is thus an essential prerequisite for interstellar-related chemistry modeling. Many distinctive features of the OH product state distributions arising from water photodissociation have already been identified and explained as exemplars of a rich gamut of nonadiabatic dynamics, for example, passage through conical intersections (CIs),<sup>4,5</sup> Coriolis couplings,<sup>6,7</sup> vibronic couplings,<sup>8</sup> and so on. Here we demonstrate another novel feature of the OH product state distribution arising in the VUV photodissociation of water, which is isotope-specific and can be attributed to an accidental vibronic resonance. Accidental resonances are often observed in molecular spectra as perturbations in line positions, intensities, or widths.<sup>9</sup> However, the effects of accidental resonances in the parent absorption on the subsequent fragmentation dynamics have rarely been recognized hitherto.

The photodissociation of H<sub>2</sub>O has been the subject of extensive experimental and theoretical investigations over the past decades, so much so that H<sub>2</sub>O (and its various

isotopomers) is now viewed as a benchmark system for illustrating and understanding nonadiabatic coupling pathways between potential energy surfaces (PESs). The excitation of H<sub>2</sub>O at  $\lambda \approx 160$  nm populates the lowest excited electronic ( $\tilde{A}^1B_1$ ) state; the subsequent direct dissociation from this state yields an H atom plus a ground-state OH( $X^2\Pi$ ) radical with little internal excitation.<sup>10–16</sup> Absorption to the second excited singlet ( $\tilde{B}^1A_1$ ) state maximizes at  $\lambda \approx 128$  nm. This state displays a minor direct dissociation channel to H + OH( $A^2\Sigma^+$ ) products and major nonadiabatic pathways via two CIs with the ground-state ( $\tilde{X}^1A_1$ ) PES at linear HOH and HHO configurations that favor the formation of highly rotationally excited OH( $X, \nu = 0$ ) products.<sup>17–29</sup> The coupling between  $\tilde{B}$  and  $\tilde{A}$  states is also possible near the linear geometry of the H<sub>2</sub>O molecule because these two states are degenerate components of a  $^1\Pi_u$  state at the linear geometry. Recently, Xie and coworkers developed the most accurate coupled PESs and provided a clear dynamical picture of water photodissociation.<sup>24–26</sup> The next two excited states identified in absorption have predominant Rydberg character and predissociate by nonadiabatic coupling to those lower (predominantly valence) states. The  $\tilde{C}^1B_1$  state shows resolvable rotational structure at  $\lambda \approx 124$  nm,<sup>30–33</sup> and previous studies

Received: June 13, 2019

Accepted: July 11, 2019

Published: July 11, 2019

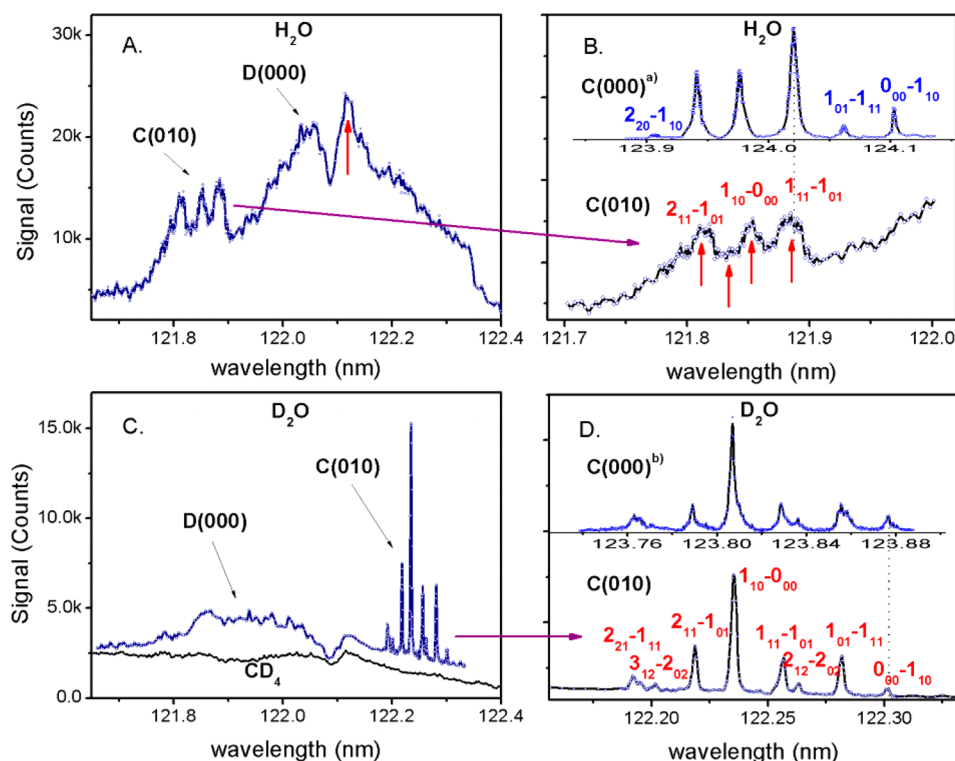


**Figure 1.** One-photon action spectra for forming (A) H atoms from  $\text{H}_2\text{O}$  and (C) D atoms from  $\text{D}_2\text{O}$  following excitation at wavelengths around 122 nm. The resolved structures at  $\lambda \approx 121.8$  nm for  $\text{H}_2\text{O}$  and  $\lambda \approx 122.2$  nm for  $\text{D}_2\text{O}$  are attributable to rotational lines of the respective  $\tilde{\text{C}}(010) \rightarrow \tilde{\text{X}}(000)$  transitions. The broad features centered at  $\lambda \approx 122.1$  nm for  $\text{H}_2\text{O}$  and  $\lambda \approx 121.9$  nm for  $\text{D}_2\text{O}$  are the respective  $\tilde{\text{D}} \leftarrow \tilde{\text{X}}$  origin bands, the profiles of which are distorted by a dip in the VUV tuning curve at  $\lambda \approx 122.09$  nm (which is also evident in the action spectrum for forming D atoms from the one-photon photolysis of  $\text{CD}_4$  shown in panel C). The extended rotational structures and line assignments of the  $\tilde{\text{C}}(010) \rightarrow \tilde{\text{X}}(000)$  transitions of  $\text{H}_2\text{O}$  and  $\text{D}_2\text{O}$  are shown in panels B and D, along with comparisons with the respective  $\tilde{\text{C}} \leftarrow \tilde{\text{X}}$  origin bands. The red arrows in panels A and B indicate the excitation wavelengths used when measuring the TKER spectra reported in Figure 4 and Figures S1 and S2.

have identified dramatic variations in the OH product state distributions and angular distributions that arise following excitation to different rotational levels of this state.<sup>34</sup> Dissociation from  $\tilde{\text{C}}$ -state rotational levels with  $K_a' = 0$  (where  $K_a$  describes the projection of the parent rotational angular momentum ( $J$ ) onto the  $a$  inertial axis) occurs exclusively by electronic coupling to the  $\tilde{\text{A}}$  state and yields highly vibrationally excited OH( $X$ ) products with vibrational quantum number  $\nu'' \leq 13$  (henceforth termed “high- $\nu$ ” products). A rival decay pathway opens for  $\text{H}_2\text{O}$  ( $\tilde{\text{C}}$ ) molecules in levels with  $K_a' > 0$ . This relies on Coriolis-type (i.e., rotationally induced) coupling to the  $\tilde{\text{B}}$ -state PES and results in both ground- ( $\tilde{\text{X}}$ ) and electronically excited-state ( $\tilde{\text{A}}$ ) OH fragments with very high rotational but minimal vibrational excitation (henceforth termed “high- $N$ ” products).

Replacing H with deuterium (D) often leads to significant isotopic effects in processes that are dynamically controlled, in particular, in cases where nonadiabatic dynamics are involved. Indeed, investigations of the photodissociation of heavy water ( $\text{D}_2\text{O}$ ) following excitation to the same excited states have revealed qualitative variations from the  $\text{H}_2\text{O}$  data but, in all cases studied to date, the same dissociation mechanisms appear to prevail for both  $\text{H}_2\text{O}$  and  $\text{D}_2\text{O}$ .<sup>35–37</sup> However, a recent ultrafast time-resolved photoelectron spectroscopy study revealed quantitatively different predissociation behaviors for the  $\tilde{\text{C}}(010)$  states (i.e., the states carrying one quantum of bending vibrational excitation,  $\nu_2'$ ) of  $\text{H}_2\text{O}$  and  $\text{D}_2\text{O}$ .<sup>38</sup> This Letter unravels the state-to-state dynamics associated with this unusual isotopic effect, using a tunable VUV pump and probe

laser sources and the high-resolution H/D-atom Rydberg tagging technique. The distinctive OH and OD quantum-state distributions determined in this work provide further exquisitely detailed illustrations of the sensitivity of the various possible nonadiabatic decay pathways to details of the excited-state PESs and the interstate coupling matrix elements.

The first experiment involved scanning the VUV photolysis wavelength while recording the total H (D) atom yield (see the [Experimental Methods in the Supporting Information](#)), thereby obtaining action spectra for forming H (D) atoms from the VUV photodissociation of  $\text{H}_2\text{O}$  ( $\text{D}_2\text{O}$ ). Figure 1A shows the action spectrum from the photolysis of  $\text{H}_2\text{O}$  in the wavelength range of 121.7 to 122.4 nm, which spans transitions to the  $\tilde{\text{C}}(010)$  state and to the origin (000) level of the  $\tilde{\text{D}}^1\text{A}_1$  state. The broad peak centered at  $\lambda \approx 122.1$  nm and extending across this entire spectral window is attributable to the  $\tilde{\text{D}} \leftarrow \tilde{\text{X}}$  origin band; the width of this feature reflects the short predissociation lifetime of the  $\tilde{\text{D}}(000)$  state.<sup>38</sup> Note that this spectrum is distorted by an obvious dip in the VUV tuning curve at  $\lambda \approx 122.09$  nm, which is also apparent in the action spectra for forming D atoms from both  $\text{D}_2\text{O}$  and  $\text{CD}_4$  photolysis, shown in Figure 1C. Analogy to the rotational fine structures of the  $\tilde{\text{C}} \leftarrow \tilde{\text{X}}$  origin band allows the partially resolved peaks at  $\lambda \approx 121.85$  nm to be assigned to the three strongest rotational lines in the jet-cooled  $\tilde{\text{C}}(010) \leftarrow \tilde{\text{X}}(000)$  transition, as shown in Figure 1B. This analysis provides an experimental estimate of the bending vibrational wavenumber for the  $\tilde{\text{C}}$  state of  $\text{H}_2\text{O}$ ,  $\nu_2' = 1402 \pm 3 \text{ cm}^{-1}$ , which is in good

accord with the values determined in previous multiphoton spectroscopy studies<sup>30</sup> and theoretical predictions.<sup>39</sup>

In contrast, the action spectrum from the photodissociation of D<sub>2</sub>O shows well-resolved rotational structure associated with the  $\tilde{C}(010) \leftarrow \tilde{X}(000)$  transition (Figure 1C). The striking similarity between this spectrum and that of the  $\tilde{C} \leftarrow \tilde{X}$  origin band (Figure 1D) allows the straightforward assignment of the rotational fine structure in the  $\tilde{C}(010) \leftarrow \tilde{X}(000)$  spectrum and yields a value of  $\nu_2' = 1040 \pm 2 \text{ cm}^{-1}$  for the  $\tilde{C}$  state of D<sub>2</sub>O. The widths of individual lines in the  $\tilde{C}(010) \leftarrow \tilde{X}(000)$  action spectra (Figure 1B,D) are  $\sim 15 \text{ cm}^{-1}$  and 1.2 to  $1.7 \text{ cm}^{-1}$  for H<sub>2</sub>O and D<sub>2</sub>O, respectively. These widths correspond to predissociation lifetimes of  $\sim 330 \text{ fs}$  for H<sub>2</sub>O and 3.0 to 4.2 ps for D<sub>2</sub>O. These are in good accord with the time-resolved measurements of He et al.<sup>38</sup> and with the conclusions from previous analyses of the respective resonance-enhanced multiphoton ionization spectra of H<sub>2</sub>O and D<sub>2</sub>O.<sup>30</sup> Such a striking isotope effect was attributed to the effects of an accidental resonance between the  $\tilde{C}(010)$  and  $\tilde{D}(000)$  vibronic levels of H<sub>2</sub>O. The  $\tilde{C}(010)$  and  $\tilde{D}(000)$  states of D<sub>2</sub>O, in contrast, are  $\sim 270 \text{ cm}^{-1}$  out of resonance,<sup>30</sup> and the mixing between the two states is thus negligible.

We have measured TOF spectra of the H (D) atom products formed with the VUV photolysis laser tuned to each of the more intense rotational lines in the  $\tilde{C}(010) \leftarrow \tilde{X}(000)$  bands of H<sub>2</sub>O and D<sub>2</sub>O. Knowing the distance traveled from the photodissociation region to the detector and the fragment masses, such time-of-flight (TOF) spectra can be converted into spectra of the total kinetic energy release (TKER). The TKER distributions obtained with the polarization vector  $\epsilon_{\text{phot}}$  aligned, respectively, parallel and perpendicular to the detection axis can then be used to construct 3-D flux diagrams of the H + OH (D + OD) fragments. Figure 2 shows such 3-D

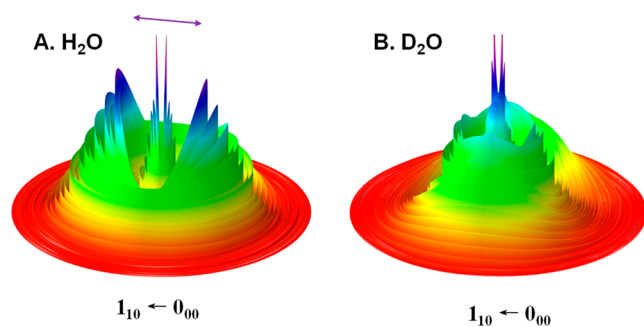


**Figure 2.** 3D contour plots of the (A) H + OH products from the photodissociation of H<sub>2</sub>O and (B) the D + OD products from the photodissociation of D<sub>2</sub>O via the  $1_{10} \leftarrow 0_{00}$  lines of the respective  $\tilde{C}(010) \leftarrow \tilde{X}(000)$  transitions. The double-headed arrow in panel A shows the alignment of  $\epsilon_{\text{phot}}$ . The outer rings in both plots are associated with the formation of rovibrational states of the ground-state (*X*) OH radical products, whereas the inner structures are primarily due to OH/OD(*A*) products.

flux diagrams for the products formed following excitation to the same  $\tilde{C}(010) \leftarrow \tilde{X}(000)$ ,  $1_{10} \leftarrow 0_{00}$  transitions of H<sub>2</sub>O and D<sub>2</sub>O. Each diagram shows two groups of features: an inner group, associated with the formation of levels of the electronically excited *A* state of OH (OD) fragments, and an outer group, associated with ground *X*-state OH (OD) products. The obvious differences in the 3-D distributions displayed in Figure 2 clearly illustrate that H<sub>2</sub>O and D<sub>2</sub>O molecules exhibit different predissociation dynamics, even

when excited via the same transition to the same  $J_{K_a K_c}$  level of the respective  $\tilde{C}(010)$  state.

Figure 3 displays TKER distributions from D<sub>2</sub>O photolysis at 122.282, 122.235, and 121.954 nm with  $\epsilon_{\text{phot}}$  aligned parallel

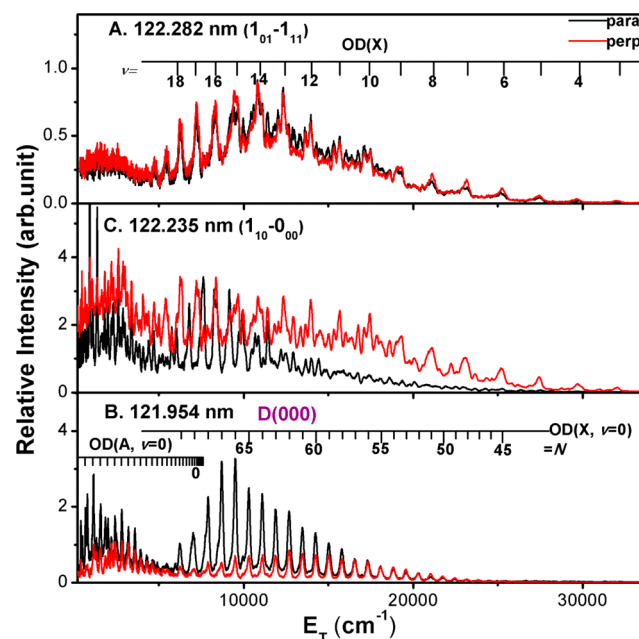


**Figure 3.** TKER spectra of the D + OD products from the photodissociation of D<sub>2</sub>O at (A) 122.282, (B) 122.235, and (C) 121.954 nm, resonant with the  $1_{01} \leftarrow 1_{11}$  and  $1_{10} \leftarrow 0_{00}$  lines of the  $\tilde{C}(010) \leftarrow \tilde{X}(000)$  transition and the center of the  $\tilde{D} \leftarrow \tilde{X}$  origin band, respectively, with  $\epsilon_{\text{phot}}$  aligned parallel (black) and perpendicular (red) to the detection axis.

and perpendicular to the detection axis. These wavelengths excite, respectively, the  $1_{01} \leftarrow 1_{11}$  and  $1_{10} \leftarrow 0_{00}$  transitions of the  $\tilde{C}(010) \leftarrow \tilde{X}(000)$  band and near the center of the  $\tilde{D} \leftarrow \tilde{X}$  origin band. All of these TKER distributions show progressions of sharp peaks. Given that the total energy and linear momentum must be conserved in the photodissociation process, we can write

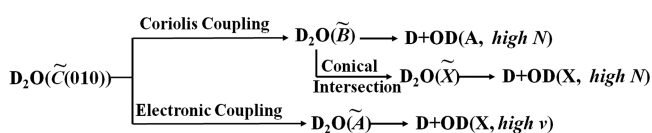
$$\begin{aligned} h\nu + E_{\text{int}}(\text{D}_2\text{O}) - D_0(\text{D} - \text{OD}) \\ = E_{\text{T}}(\text{D} + \text{OD}) + E_{\text{int}}(\text{OD}) \end{aligned} \quad (1)$$

where the internal energy ( $E_{\text{int}}$ ) distribution of the OD fragment can be determined from the TKER ( $E_{\text{T}}$ ) distribution,  $h\nu$  is the photolysis photon energy,  $h$  is Planck's constant, and  $D_0(\text{D} - \text{OD})$  is the bond dissociation energy. In the supersonic expansion, the water molecule is cooled to a very low temperature, suggesting that  $E_{\text{int}}(\text{D}_2\text{O}) \approx 0$ . All of the sharp peaks in Figure 3 can be assigned to the population of specific rovibrational levels of the *A* and *X* states of OD.

The excited level populated at the first of these wavelengths has  $K_a' = 0$ , and, as Figure 3A shows, the TKER spectrum is invariant to the alignment of  $\epsilon_{\text{phot}}$  (i.e., the recoil velocity distribution is isotropic) and the fine structure indicates that the OD products are formed in their ground (*X*) state, in very widespread of vibrational states (up to  $v'' = 18$ ), and with little rotational excitation. Both the energy disposal and the isotropy of the product recoil are very similar to those found when exciting the same rotational transition within the  $\tilde{C}(000) \leftarrow \tilde{X}(000)$  origin band<sup>36</sup> but totally different from that observed

when exciting to the  $\tilde{D}(000)$  state, which yields high- $N$  OD products (Figure 3C). The TKER spectra obtained following the excitation of the  $1_{10} \leftarrow 0_{00}$  transition (i.e., populating a  $\tilde{C}(010)$ -state level with  $K_a' = 1$ ) are different again. As Figure 3B shows, the spectrum recorded in the perpendicular direction is dominated by high- $\nu$  OD( $X$ ) products, whereas high- $N$  OD ( $A$ ) and OD( $X$ ) products dominate the TKER spectrum recorded in the parallel direction. Again, these very obvious differences are reminiscent of those previously reported when exciting the same rotational transition in the  $\tilde{C} \leftarrow \tilde{X}$  origin band of  $D_2O$  (and  $H_2O$ ).<sup>34,36</sup> These parallels suggest that the predissociation of  $\tilde{C}(010)$ - and  $\tilde{C}(000)$ -state  $D_2O$  molecules follows essentially the same mechanisms, namely, a Coriolis-induced pathway to the  $\tilde{B}$ -state PES and an electronic coupling to the  $\tilde{A}$ -state PES, as summarized in Scheme 1. (It is noted that the direct route from  $\tilde{C} \rightarrow \tilde{A}$  is

Scheme 1



minor, and the major route follows  $\tilde{C} \rightarrow {}^1A_2 \rightarrow \tilde{A}^8$ ). The former yields high- $N$  OD( $X$ ) and OD( $A$ ) products, whereas the latter yields high- $\nu$  OD( $X$ ) products. The products of these two pathways show opposite recoil anisotropies, and, for  $\tilde{C}(010)$  levels with  $K_a' = 1$ , the respective signals suggest that the two processes occur with comparable efficiencies.

The situation with  $H_2O$  is very different. Figure 4 shows the TKER distributions obtained when exciting each of the three  $\tilde{C}(010) \leftarrow \tilde{X}(000)$  transitions identified in Figure 1B. TKER

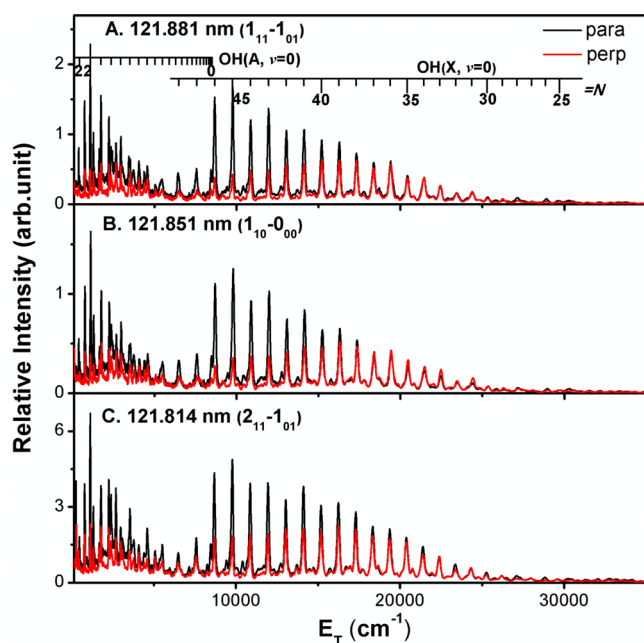


**Figure 4.** TKER spectra of the H + OH products from the photodissociation of  $H_2O$  at (A) 121.881, (B) 121.851, and (C) 121.814 nm, resonant with the  $1_{11} \leftarrow 1_{01}$ ,  $1_{10} \leftarrow 0_{00}$ , and  $2_{11} \leftarrow 1_{01}$  rotational lines of the  $\tilde{C}(010) \leftarrow \tilde{X}(000)$  transition, respectively, with  $\epsilon_{\text{phot}}$  aligned parallel (black) and perpendicular (red) to the detection axis.

distributions were also measured with the photolysis wavelength tuned to the valley between the peaks at 121.851 and 121.814 nm in the action spectrum and to 122.117 nm (where absorption is ascribed exclusively to the  $\tilde{D} \leftarrow \tilde{X}$  origin transition). These are shown in the Supporting Information (Figures S1 and S2). The TKER distributions obtained at all five wavelengths are essentially identical, showing progressions of sharp peaks that can be assigned to the population of high- $N$  levels of the  $A$  and  $X$  states of OH.

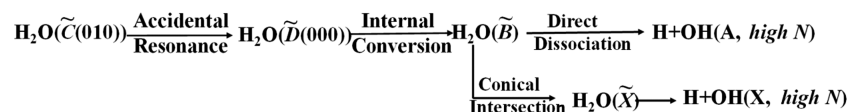
The TKER distributions and the recoil anisotropies appear insensitive to whether the initial excitation is to any of the three  $\tilde{C}(010)$ -state rotational levels or to the  $\tilde{D}(000)$  state. Note that each of the probed  $\tilde{C}(010)$  levels of  $H_2O$  has  $K_a' = 1$  (and thus  $\langle J_a^2 \rangle = 1$ ). Unfortunately, the line strengths of the  $0_{00} \leftarrow 1_{10}$  and  $1_{01} \leftarrow 1_{11}$  transitions (which populate levels with  $\langle J_a^2 \rangle = 0$ ) are too weak to be identified under the stronger  $\tilde{D} \leftarrow \tilde{X}$  origin band, and any transitions to levels with  $K_a' = 2$  are too heavily predissociated to be resolved.<sup>30</sup> What is immediately obvious, however, is that in contrast with  $D_2O$ , the fragmentation of  $H_2O$   $\tilde{C}(010)$  molecules with  $K_a' = 1$  yields high- $N$  products; that is, the fragmentation dynamics are indicative of the eventual nuclear motion on the  $\tilde{B}$ -state PES, which is different from that when exciting the same rotational transition within the  $\tilde{C}(000) \leftarrow \tilde{X}(000)$  origin band (Figures S3). The TKER spectra in the perpendicular direction show no indication of any high- $\nu$  OH( $X$ ) products, such as would be expected if nonadiabatic coupling from these levels to the  $\tilde{A}$ -state PES was a competitive process.

The striking isotope-dependent dynamics of the  $\tilde{C}(010)$ ,  $K_a' = 1$  levels of  $H_2O$  are directly attributable to the accidental resonance between the  $\tilde{C}(010)$  and  $\tilde{D}(000)$  states of  $H_2O$ . As noted above, the  $\tilde{D}$  and  $\tilde{B}$  states share a common ( ${}^1A_1$ ) symmetry, and the  $\tilde{D}(000)$  states of both isotopomers are efficiently predissociated by electronic mixing with the  $\tilde{B}$ -state continuum. The  $\tilde{C}$  state, in contrast, has  ${}^1B_1$  symmetry. As shown in Scheme 1,  $\tilde{C}$ -state molecules can decay by electronic (same symmetry) coupling to the  $\tilde{A}$ -state continuum or, if prepared with appropriate nuclear motion ( $a$ -axis rotation), by coupling to the  $\tilde{B}$ -state continuum. The two decay pathways have comparable probabilities for  $D_2O$  molecules, with  $K_a' = 1$  in either the  $\tilde{C}(000)$  or  $\tilde{C}(010)$  states, and for  $H_2O$ ,  $\tilde{C}(000)$  molecules with  $K_a' = 1$ . However, the accidental resonance with the  $\tilde{D}(000)$  state greatly boosts the efficiency of Coriolis coupling from the  $\tilde{C}(010)$  state,  $K_a' = 1$  levels of  $H_2O$  to the  $\tilde{B}$ -state continuum, as illustrated in Scheme 2, to the extent that this pathway to high- $N$  products overwhelms the potential rival electronic coupling route to high- $\nu$  OH( $X$ ) products.

A further feature of the OH( $X$ ,  $\nu = 0$ ) rotational distributions displayed in Figure 4 is the clear intensity alternation in the populations of successive  $N$  levels. These alternations are reminiscent of those observed in the OH( $X$ ) fragments arising in the 121.6 nm photolysis of  $H_2O$ <sup>5</sup> and, as in that case, can be attributed to dynamical interferences between dissociation pathways via the CIs between the  $\tilde{B}$ - and  $\tilde{X}$ -state PESs at linear H–O–H and H–H–O geometries.

The dissociation mechanisms shown in Schemes 1 and 2 highlight a clear yet unprecedented isotope dependence in the photodissociation of  $\tilde{C}(010)$ -state water molecules. Previous studies have revealed qualitatively different dissociation behaviors for  $H_2O$  and  $D_2O$  molecules following the excitation to the same electronic states, and most of these effects could be attributed to mass changes.<sup>35–37</sup> Here we reveal a much more dramatic isotope effect caused by accidental resonance, which

Scheme 2



leads to different dissociation rates, different dissociation mechanisms, and different product energy disposals following excitation to a common excited state of H<sub>2</sub>O and D<sub>2</sub>O. Given the high density of excited vibronic levels of H<sub>2</sub>O and D<sub>2</sub>O accessible at shorter excitation wavelengths,<sup>40</sup> it would be surprising if the accidental resonance and the striking isotope-dependent fragmentation dynamics—identified in the present study were to be the only example available following VUV photoexcitation of water molecules.

The photodissociation of water is invoked as an important photochemical process in interstellar molecular clouds.<sup>41</sup> Thus the isotope-specific dissociation process identified in the present study may have implications in modeling chemistry prevailing in the ISM. For example, self-shielding has been proposed to account for the observed isotope heterogeneity within the solar system,<sup>42,43</sup> but recent investigations of the VUV photodissociation of CO support the view that perturbation-dominated state-mixing dynamics will also introduce isotopologue-dependent dissociation probabilities.<sup>44,45</sup> The strikingly different fragmentation dynamics of H<sub>2</sub>O and D<sub>2</sub>O observed in the present work represent an extreme example of such accidental-resonance-induced state mixing and may be expected to contribute to the D/H isotope heterogeneity in the solar system.

In summary, detailed dynamical features of the photodissociation of  $\tilde{\text{C}}(010)$ -state H<sub>2</sub>O and D<sub>2</sub>O molecules have been determined using a tunable VUV source in combination with the high-resolution H/D-atom Rydberg tagging technique. The predissociation mechanisms of H<sub>2</sub>O and D<sub>2</sub>O following the excitation to the  $\tilde{\text{C}}(010)$  state show a striking isotopologue dependence. The OH product state distributions are determined by the accidental-resonance-mediated non-adiabatic coupling pathway, but this pathway has a negligible influence on the OD product state distributions. The present study provides an excellent example of competitive state-to-state nonadiabatic couplings and decay pathways involving at least five electronic PESs.

## ■ ASSOCIATED CONTENT

### Supporting Information

The Supporting Information is available free of charge on the ACS Publications website at DOI: 10.1021/acs.jpcl.9b01710.

Detailed description of the experimental methods, Figures S1–S3, and references (PDF)

## ■ AUTHOR INFORMATION

### Corresponding Authors

\*E-mail: wugr@dicp.ac.cn (G.W.)

\*E-mail: kiyuan@dicp.ac.cn (K.Y.)

\*E-mail: xmyang@dicp.ac.cn (X.Y.)

### ORCID

Guorong Wu: 0000-0002-0212-183X

Michael N. R. Ashfold: 0000-0001-5762-7048

Kaijun Yuan: 0000-0002-5108-8984

## Author Contributions

<sup>§</sup>Y.C. and Z.C. contributed equally.

## Notes

The authors declare no competing financial interest.

## ■ ACKNOWLEDGMENTS

The experimental work is supported by the National Natural Science Foundation of China (NSFC nos. 21873099, 21673232), the Strategic Priority Research Program of the Chinese Academy of Sciences (grant no. XDB 17000000), and the Chemical Dynamics Research Center (grant no. 21688102). M.N.R.A. gratefully acknowledges funding from the Engineering and Physical Sciences Research Council (EPSRC, EP/L005913) and the NSFC Center for Chemical Dynamics for the award of a Visiting Fellowship. Z.C. is supported by the National Natural Science Foundation of China (NSFC no. 21773236). G.W. acknowledges funding from the State Key Program of National Natural Science Foundation of China (grant no. 21833003).

## ■ REFERENCES

- Lee, L. C.; Suto, M. Quantitative Photoabsorption and Fluorescence Study of H<sub>2</sub>O and D<sub>2</sub>O at 50–190 nm. *Chem. Phys.* **1986**, *110*, 161–169.
- Carr, J. S.; Najita, J. R. The OH Rotational Population and Photodissociation of H<sub>2</sub>O in DG Tauri. *Astrophys. J.* **2014**, *788*, 66.
- Chang, Y.; Yu, Y.; Wang, H. L.; Hu, X. X.; Li, Q. M.; Yang, J. Y.; Su, S.; He, Z. G.; Chen, Z. C.; Che, L.; Wang, X. N.; Zhang, W. Q.; Wu, G. R.; Xie, D. Q.; Ashfold, M. N. R.; Yuan, K. J.; Yang, X. M. Hydroxyl Super Rotors from Vacuum Ultraviolet Photodissociation of Water. *Nat. Commun.* **2019**, *10*, 1025.
- Dixon, R. N.; Hwang, D. W.; Yang, X. F.; Harich, S.; Lin, J. J.; Yang, X. Chemical "Double Slits": Dynamical Interference of Photodissociation Pathways in Water. *Science* **1999**, *285*, 1249–1253.
- Harich, S. A.; Yang, X. F.; Hwang, D. W. H.; Lin, J. J.; Yang, X. M.; Dixon, R. N. Photodissociation of D<sub>2</sub>O at 121.6 nm: A State-to-state Dynamical Picture. *J. Chem. Phys.* **2001**, *114*, 7830–7837.
- Yuan, K. J.; Dixon, R. N.; Yang, X. M. Photochemistry of the Water Molecule: Adiabatic versus Nonadiabatic Dynamics. *Acc. Chem. Res.* **2011**, *44*, 369–378.
- Hwang, D. W.; Yang, X. F.; Harich, S.; Lin, J. J.; Yang, X. Photodissociation Dynamics of H<sub>2</sub>O at 121.6 nm: Effect of Parent Rotational Excitation on Reaction Pathways. *J. Chem. Phys.* **1999**, *110*, 4123–4126.
- Dixon, R. N.; Oliver, T. A. A.; Cheng, L.; Cheng, Y.; Yuan, K. J.; Yang, X. M. Vibronically Induced Decay Paths from the  $\tilde{\text{C}}^1\text{B}_1$ -state of Water and Its Isotopomers. *J. Chem. Phys.* **2013**, *138*, 104306.
- Herzberg, G. *Electronic Spectra of Polyatomic Molecules*; Van Nostrand: Princeton, NJ, 1966.
- Engel, V.; Schinke, R.; Staemmler, V. Photodissociation Dynamics of H<sub>2</sub>O and D<sub>2</sub>O in the First Absorption Band - A Complete Ab Initio Treatment. *J. Chem. Phys.* **1988**, *88*, 129–148.
- Guo, H.; Murrell, J. N. Dynamics of the A-state Photodissociation of H<sub>2</sub>O at 193 nm. *Mol. Phys.* **1988**, *65*, 821–827.
- Engel, V.; Staemmler, V.; Vanderwal, R. L.; Crim, F. F.; Sension, R. J.; Hudson, B.; Andresen, P.; Hennig, S.; Weide, K.; Schinke, R. Photodissociation of Water in the First Absorption Band - A Prototype for Dissociation on a Repulsive Potential Energy Surface. *J. Phys. Chem.* **1992**, *96*, 3201–3213.

- (13) Yang, X. F.; Hwang, D. W.; Lin, J. J.; Ying, X. M. Dissociation Dynamics of the Water Molecule on the  $\tilde{A}^1B_1$  Electronic Surface. *J. Chem. Phys.* **2000**, *113*, 10597–10604.
- (14) van Harrevelt, R.; van Hemert, M. C. Photodissociation of Water in the  $\tilde{A}$  Band Revisited with New Potential Energy Surfaces. *J. Chem. Phys.* **2001**, *114*, 9453–9462.
- (15) Zhou, L. S.; Xie, D. Q.; Sun, Z. G.; Guo, H. Product Fine-structure Resolved Photodissociation Dynamics: The  $\tilde{A}$  Band of  $H_2O$ . *J. Chem. Phys.* **2014**, *140*, No. 024310.
- (16) Lu, I. C.; Wang, F. Y.; Yuan, K. J.; Cheng, Y.; Yang, X. M. Nonstatistical Spin Dynamics in Photodissociation of  $H_2O$  at 157 nm. *J. Chem. Phys.* **2008**, *128*, No. 066101.
- (17) van Harrevelt, R.; van Hemert, M. C. Photodissociation of Water. I. Electronic Structure Calculations for the Excited States. *J. Chem. Phys.* **2000**, *112*, 5777–5786.
- (18) van Harrevelt, R.; van Hemert, M. C. Photodissociation of Water. II. Wave Packet Calculations for the Photofragmentation of  $H_2O$  and  $D_2O$  in the  $\tilde{B}$  Band. *J. Chem. Phys.* **2000**, *112*, 5787–5808.
- (19) Fillion, J. H.; van Harrevelt, R.; Ruiz, J.; Castillejo, N.; Zanganeh, A. H.; Lemaire, J. L.; van Hemert, M. C.; Rostas, F. Photodissociation of  $H_2O$  and  $D_2O$  in  $\tilde{B}$ ,  $\tilde{C}$ , and  $\tilde{D}$  States (134–119 nm). Comparison between Experiment and Ab Initio Calculations. *J. Phys. Chem. A* **2001**, *105*, 11414–11424.
- (20) Mordaunt, D. H.; Ashfold, M. N. R.; Dixon, R. N. Dissociation Dynamics of  $H_2O$  ( $D_2O$ ) Following Photoexcitation at the Lyman- $\alpha$  Wavelength (121.6 nm). *J. Chem. Phys.* **1994**, *100*, 7360–7375.
- (21) Cheng, Y.; Yuan, K. J.; Cheng, L. N.; Guo, Q.; Dai, D. X.; Yang, X. M. Photodissociation Dynamics of  $H_2O$ : Effect of Unstable Resonances on the  $\tilde{B}^1A_1$  Electronic State. *J. Chem. Phys.* **2011**, *134*, No. 064301.
- (22) Vondirke, M.; Heumann, B.; Kuhl, K.; Schroder, T.; Schinke, R. Fluctuations in Absorption Spectra and Final Product State Distributions following Photodissociation Processes. *J. Chem. Phys.* **1994**, *101*, 2051–2068.
- (23) Zhou, L. S.; Jiang, B.; Xie, D. Q.; Guo, H. State-to-state Photodissociation Dynamics of  $H_2O$  in the  $\tilde{B}$  Band: Competition between Two Coexisting Nonadiabatic Pathways. *J. Phys. Chem. A* **2013**, *117*, 6940–6947.
- (24) Zhou, L. S.; Lin, G. S. M.; Xie, D. Q. State to State Photodissociation Dynamics of  $D_2O$  in the  $\tilde{B}$  Band. *J. Chem. Phys.* **2013**, *139*, 114303.
- (25) Jiang, B.; Xie, D. Q.; Guo, H. State-to-state Photodissociation Dynamics of Triatomic Molecules:  $H_2O$  in the  $\tilde{B}$  Band. *J. Chem. Phys.* **2012**, *136*, No. 034302.
- (26) Hu, X. X.; Zhou, L. S.; Xie, D. Q. State-to-state Photodissociation Dynamics of the Water Molecule. *Wires Comput. Mol. Sci.* **2018**, *8*, e1350.
- (27) Su, S.; Wang, H. Z.; Chen, Z. C.; Yu, S. R.; Dai, D. X.; Yuan, K. J.; Yang, X. M. Photodissociation Dynamics of HOD via the  $\tilde{B}^1A_1$  Electronic State. *J. Chem. Phys.* **2015**, *143*, 184302.
- (28) Yi, W. K.; Park, J.; Lee, J. Photodissociation Dynamics of Water at Lyman- $\alpha$  (121.6 nm). *Chem. Phys. Lett.* **2007**, *439*, 46–49.
- (29) Zanganeh, A. H.; Fillion, J. H.; Ruiz, J.; Castillejo, M.; Lemaire, J. L.; Shafizadeh, N.; Rostas, F. Photodissociation of  $H_2O$  and  $D_2O$  below 132 nm. *J. Chem. Phys.* **2000**, *112*, 5660–5671.
- (30) Ashfold, M. N. R.; Bayley, J. M.; Dixon, R. N. Molecular Predissociation Dynamics Revealed through Multiphoton Ionization Spectroscopy. I. The  $\tilde{C}^1B_1$  States of  $H_2O$  and  $D_2O$ . *Chem. Phys.* **1984**, *84*, 35–50.
- (31) Kuge, H. H.; Kleiner, K. Rotational Predissociation of  $H_2O$  ( $\tilde{C}^1B_1$ ) Studied by Multiphoton Ionization Spectroscopy in a Supersonic Free Jet. *J. Chem. Phys.* **1989**, *90*, 46–52.
- (32) Hodgson, A.; Simons, J. P.; Ashfold, M. N. R.; Bayley, J. M.; Dixon, R. N. Quantum State-selected Photodissociation Dynamics in  $H_2O$  and  $D_2O$ . *Mol. Phys.* **1985**, *54*, 351–368.
- (33) Yang, C. H.; Sarma, G.; ter Meulen, J. J.; Parker, D. H.; Western, C. M. REMPI Spectroscopy and Predissociation of the  $\tilde{C}^1B_1$  ( $\nu = 0$ ) Rotational Levels of  $H_2O$ , HOD and  $D_2O$ . *Phys. Chem. Chem. Phys.* **2010**, *12*, 13983–13991.
- (34) Yuan, K. J.; Cheng, Y.; Cheng, L.; Guo, Q.; Dai, D. X.; Wang, X. Y.; Yang, X. M.; Dixon, R. N. Nonadiabatic Dissociation Dynamics in  $H_2O$ : Competition between Rotationally and Nonrotationally Mediated Pathways. *Proc. Natl. Acad. Sci. U. S. A.* **2008**, *105*, 19148–19153.
- (35) Harich, S. A.; Yang, X. F.; Hwang, D. W. H.; Lin, J. J.; Yang, X. M.; Dixon, R. N. Photodissociation of  $D_2O$  at 121.6 nm: A State-to-state Dynamical Picture. *J. Chem. Phys.* **2001**, *114*, 7830–7837.
- (36) Cheng, Y.; Cheng, L. N.; Guo, Q.; Yuan, K. J.; Dai, D. X.; Wang, X. Y.; Dixon, R. N.; Yang, X. M. Rotational State Specific Dissociation Dynamics of  $D_2O$  via the  $\tilde{C}$  Electronic State. *J. Chem. Phys.* **2010**, *133*, No. 034307.
- (37) Cheng, Y.; Cheng, L. N.; Guo, Q.; Yuan, K. J.; Dai, D. X.; Yang, X. M. Photodissociation Dynamics of  $D_2O$  via the  $\tilde{B}^1A_1$  Electronic State. *J. Chem. Phys.* **2011**, *134*, 104305.
- (38) He, Z. G.; Yang, D. Y.; Chen, Z. C.; Yuan, K. J.; Dai, D. X.; Wu, G. R.; Yang, X. M. An Accidental Resonance Mediated Predissociation Pathway of Water Molecules Excited to the Electronic  $\tilde{C}$  State. *Phys. Chem. Chem. Phys.* **2017**, *19*, 29795–29800.
- (39) Johns, J. W. C. On the Absorption Spectrum of  $H_2O$  and  $D_2O$  in Vacuum Ultraviolet. *Can. J. Phys.* **1963**, *41*, 209–219.
- (40) Fillion, J. H.; Ruiz, J.; Yang, X. F.; Castillejo, M.; Rostas, F.; Lemaire, J. L. High resolution photoabsorption and photofragment fluorescence spectroscopy of water between 10.9 and 12 eV. *J. Chem. Phys.* **2004**, *120*, 6531–6541.
- (41) Van Dishoeck, E. F.; Herbst, E.; Neufeld, D. A. Interstellar Water Chemistry: From Laboratory to Observations. *Chem. Rev.* **2013**, *113*, 9043–9085.
- (42) Yurimoto, H.; Kuramoto, K. Molecular Cloud Origin for the Oxygen Isotope Heterogeneity in the Solar System. *Science* **2004**, *305*, 1763–1766.
- (43) Lyons, J. R.; Young, E. D. CO Self-shielding as the Origin of Oxygen Isotope Anomalies in the Early Solar Nebula. *Nature* **2005**, *435*, 317–320.
- (44) Chakraborty, S.; Rude, B.; Ahmed, M.; Thieme, M. H. Carbon and Oxygen Isotopic Fractionation in the Products of Low-temperature VUV Photodissociation of Carbon Monoxide. *Chem. Phys.* **2018**, *514*, 78–86.
- (45) Chakraborty, S.; Ahmed, M.; Jackson, T. L.; Thieme, M. H. Experimental Test of Self-shielding in Vacuum Ultraviolet Photodissociation of CO. *Science* **2008**, *321*, 1328–1331.